ACS APPLIED MATERIALS & INTERFACES

Research Article

www.acsami.org

A Lithographically Patterned Capacitor with Horizontal Nanowires of Length 2.5 mm

Wenbo Yan,[†] Mya Le Thai,[†] Rajen Dutta,[‡] Xiaowei Li,[‡] Wendong Xing,[‡] and Reginald M. Penner*[,†,¶]

[†]Department of Chemistry, University of California, Irvine, California 92697-2025, United States

[‡]Department of Physics and Astronomy, University of California, Irvine, California 92697, United States

[¶]Department of Chemical Engineering and Materials Science, University of California, Irvine, California 92697-2700, United States

ABSTRACT: A symmetrical hybrid capacitor consisting of interdigitated, horizontal nanowires is described. Each of the 750 nanowires within the capacitor is 2.5 mm in length, consisting of a gold nanowire core (40 × ≈200 nm) encapsulated within a hemicylindrical shell of δ-phase MnO_2 (thickness = 60−220 nm). These Au@δ-MnO_2 nanowires are patterned onto a planar glass surface using lithographically patterned nanowire electrodeposition (LPNE). A power density of 165 kW/kg and energy density of 24 Wh/kg were obtained for a typical nanowire array in which the MnO_2 shell thickness was 68 ± 8 nm. Capacitors incorporating these ultralong nanowires lost ≈10% of their capacity rapidly, during the first 20 discharge cycles, and then retained 90% of their maximum capacity for the ensuing 6000 cycles. The ability of capacitors consisting of ultralong Au@δ-MnO_2 nanowires to simultaneously deliver high power and high capacity with acceptable cycle life is demonstrated.

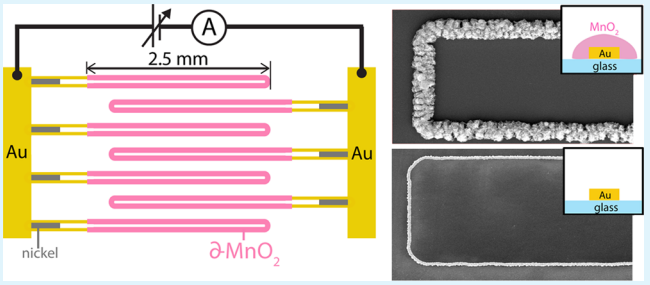

KEYWORDS: *electrochemical capacitors, lithium ion, manganese oxide, electrodeposition, photolithography, pseudo-capacitance*

Hybrid electrochemical capacitors (ECs)[1−3] can generate high power (>10^3 W/kg) like true capacitors while also having the high specific energy (>10 Wh/kg) characteristic of batteries.[3] Hybrid ECs achieve this feat by exploiting two mechanisms for storing electrical energy: (1) A non-Faradaic capacity derived from double-layer charging, like true electrochemical capacitors, and (2) a Faradaic capacity derived from changes in the redox state of the material, like batteries.[1−3] MnO_2, for example, has an electrical conductivity that is high enough to require double-layer charging[4] and it is able to access changes in Mn redox state providing a mechanism for a Faradaic pseudo-capacitance (for reviews, see refs 5−8)

$$MnO_2 + X^+(aq) + e^- \leftrightarrow MnOOX \quad (1)$$

Reaction 1 can occur both at Mn centers located in the bulk of the material, in which case the insertion of X^+ to compensate charge is required, and also at Mn centers located at the surface of the MnO_2 where solvated X^+ can compensate charge without inserting.

The driving force for investigating MnO_2 materials with a critical dimension, d_c, in the nanometer regime is two-fold: First, the wetted surface area of the material is increased as d_c is reduced, increasing both the double-layer capacity and the noninsertion Faradaic capacity. Second, the maximum distance over which charge compensating cations, X^+, must move in the solid is equal to $0.5d_c$, so reducing d_c increases both charge−discharge rates and the specific capacities for these materials.[6−8] With these motivations, MnO_x nanowires have been synthesized by many research groups who have also reported their electrochemical charge storage properties. For example, Jiang et al.[9] prepared single crystalline, β-phase MnO_2 nanowires as small as ∼3−7 nm in diameter. These nanowires produced specific capacities, C_{sp}, of 279 F/g for constant current discharge at 1 A/g and 170 F/g for voltammetric cycling at 50 mV/s.[9] Somewhat higher C_{sp} values have been reported for template-synthesized nanotubes of polycrystalline MnO_2 (349[10] and 493 F/g[11]), whereas single crystalline MnO_2 nanotubes had a somewhat lower C_{sp} (220 F/g).[12] α-Phase MnO_2 nanorods with diameters of 20−50 nm produced a maximum C_{sp} of 233 F/g.[13]

We have used lithographically patterned nanowire electrodeposition (LPNE)[14−16] to prepare mesoporous δ-MnO_2 nanowires of two types.[17,18] In our initial work,[17] arrays of 20 nm × 400 nm *mp*-MnO_2 nanowires produced a specific capacitance C_{sp} ≈ 900 F/g at 5 mV/s and ≈400 F/g at 100 mV/s.[17] These C_{sp} values compare favorably with the highest seen previously for this material;[17] but to achieve this performance, the high Ohmic resistance of the MnO_2 had to be mitigated by using a macroscopic gold film as a current collector for the MnO_2 nanowires along their entire lengths. Subsequently,[18] we prepared nanowires consisting of a gold nanowire core (40 × ≈200 nm) covered with a shell of δ-phase MnO_2 (thickness = 60−220 nm). These Au@δ-MnO_2 nanowires showed both a high specific capacity of 1020 ±

Received: January 3, 2014
Accepted: March 12, 2014
Published: March 12, 2014

100 F/g at 5 mV/s and 450 ± 70 F/g at 100 mV/s coupled with retention of this capacity to 1000 charge/discharge cycles.

Here, we explore the feasibility of fabricating a symmetrical, all nanowire capacitor based upon arrays of 750 Au@δ-MnO_2 nanowires that are each 2.5 mm in total length (Figure 1a).

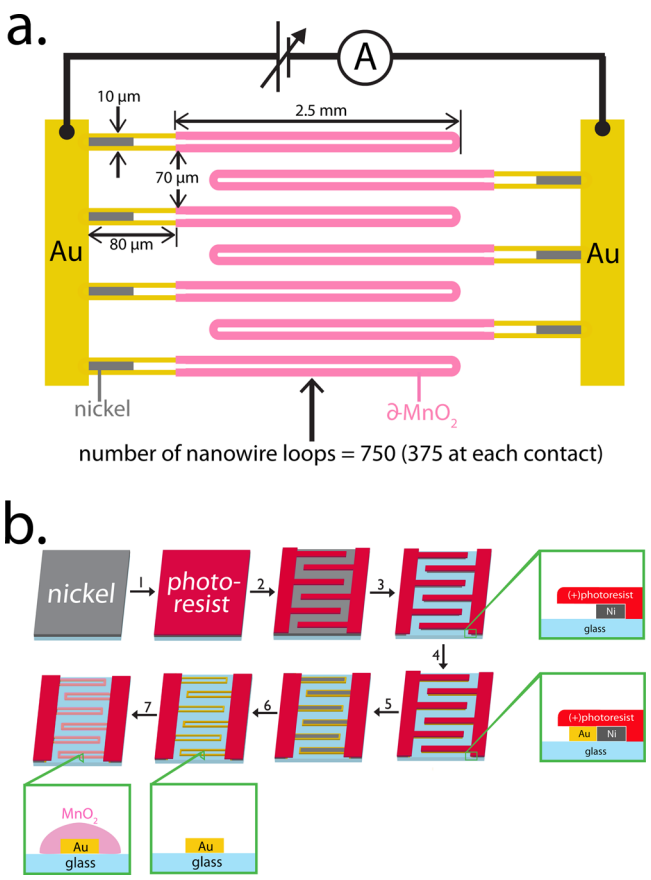

Figure 1. (a) Schematic diagram of the symmetrical horizontal interdigitated MnO_2@Au nanowire array showing wire lengths and displacements. (b) Process flow for the fabrication of this device using the lithographically patterned nanowire electrodeposition (LPNE) method.

These nanowires are lithographically patterned in an interdigitated pattern onto glass (Figure 1ab), lifting the requirement for a separator. From a reliability standpoint, ultralong nanowires actually constitute a critical *disadvantage* for the following reason: The sensitivity of the capacity to degradation processes that culminate in nanowire breakage increases with the nanowire length (Figure 2). Specifically, if one considers an array of 10 nanowires of length one unit, the removal of one nanowire by a single break-inducing defect can reduce the capacity by, at most, 1 unit (or 10% of 10 units, Figure 2a). For an array of nanowires that are twice as long, a single break can reduce the total capacity of the electrode by up to 2 units (or 20% of 10 units, Figure 2b). In other words, a single nanowire breakage "disconnects" more capacity from the device as the length of individual nanowires within the device increases, provided the total length of nanowires in the device is constant (Figure 2c). Beyond nanowire scission, other possible failure modes for these nanowires include delamination of the MnO_2 shell from the gold nanowire core and dissolution of the MnO_2, facilitated by Mn^{3+} disproportionation.[9,10,19]

The goal of this project was to probe the stability of millimeter-scale Au@δ-MnO_2 nanowires and to directly measure the charge storage metrics of capacitors based upon these structures. Surprisingly, despite the predicted sensitivity of long nanowires to degradation processes, we demonstrate here that state-of-the-art charge storage metrics and superb cycle stability can be achieved using these systems. Specifically, interdigitated supercapacitors show a maximum power density of 165 kW/kg coupled with an energy density of 24 Wh/kg for a Au/MnO_2 nanowire with the MnO_2 shell thickness of 68 nm. Cycle stability to 6000 times at 100 mV/s across a 1.2 V window is demonstrated. These data support the conclusion that durable, ultrahigh power density capacitors can be fabricated based upon millimeter-scale metal core−metal oxide shell nanowire arrays.

EXPERIMENTAL SECTION

Chemicals and Materials. Manganese perchlorate hydrate ($Mn(ClO_4)_2{\cdot}H_2O$, 99%), lithium perchlorate ($LiClO_4$, 95%), and iodine (I_2, 99.8%) were used as received from Sigma-Aldrich. Sulfuric acid (ULTREX ultrapure) was purchased from J. T. Baker. Potassium iodide (KI, 99%), acetone, methanol, and nitric acid were used as received from Fisher (ACS Certified). Positive photoresists, Shipley S-1808 and developer MF-319 were purchased from Microchem Corporation.

Preparation of Interdigitated Au@δ-MnO_2 Core@Shell Nanowires. Au@δ-MnO_2 nanowire arrays were prepared by electrodeposition using the LPNE process shown in Figure 1b.[14−16] A 40 nm thick film of nickel was thermally evaporated on precleaned 1″ × 1″ squares of soda lime glass. Then (Figure 1b, step 1), a positive photoresist (PR, Shipley, S1808) layer was deposited by spin-coating, followed by soft-baking at 90 °C for 30 min, and (Figure 1b, step 2) a contact mask was used to pattern this PR layer with a 365 nm UV light source combined with a shutter and alignment stage (Newport, 83210i-line, 1.80s). After developing the patterned PR region for 15 s (Shipley, MF-319) and rinsing with Millipore water (Mill-Q, ρ > 18 MΩ cm), the exposed nickel was removed by etching in 0.80 M nitric acid for 7 min to produce a horizontal trench with a typical width of 300 nm (Figure 1b, step 3).

Gold nanowires were then electrodeposited by immersing the patterned chip into commercial Au plating solution (Clean Earth Solutions) (Figure 1b, step 4). This electrodeposition was potentiostatic at −0.90 V vs saturated calomel electrode (SCE) using a Princeton Applied Research 2263 potentiostat in conjunction with a one-compartment three-electrode electrochemical cell with a Pt foil counter electrode. After electrodeposition of the gold nanowires, the chip was rinsed with acetone to remove photoresist, revealing patterned Ni fingers that are edged with gold nanowires (Figure 1b, step 5). A second photoresist layer was then spin-coated onto the device. A rectangular contact mask was used to pattern the PR layer to expose the Ni contact. Nickel was then removed by immersion into nitric acid for 6 min (Figure 1b, step 6). After etching, the device, now consisting of isolated gold nanowire loops on glass, was rinsed with Millipore water and air-dried. The device was placed into a 250 °C oven and hard-baked, rending the photoresist impervious to acetone. Using these gold nanowires as the working electrode, δ-MnO_2 was electrodeposited potentiostatically at +0.6 V versus saturated mercurous sulfate reference electrode (MSE) for 1−5 s, producing a hemicylindrical shell of δ-MnO_2 on the gold nanowires (Figure 1b, step 7).[20] The plating solution utilized for MnO_2 growth was aqueous 2 mM $Mn(ClO_4)_2$, 50 mM $LiClO_4$.[15] When the deposition was completed, the glass slide was removed from the plating solution, rinsed with Millipore water, and dried in the oven at 90 °C for 30 min prior to electrochemical assessment. This process created the "Au@δ-MnO_2 core@shell nanowires" that consisted of a Au nanowire as the core and a shell composed of δ-MnO_2 .

Electrochemical Characterization. All electrodeposition experiments were performed by a one-compartment three-electrode cell

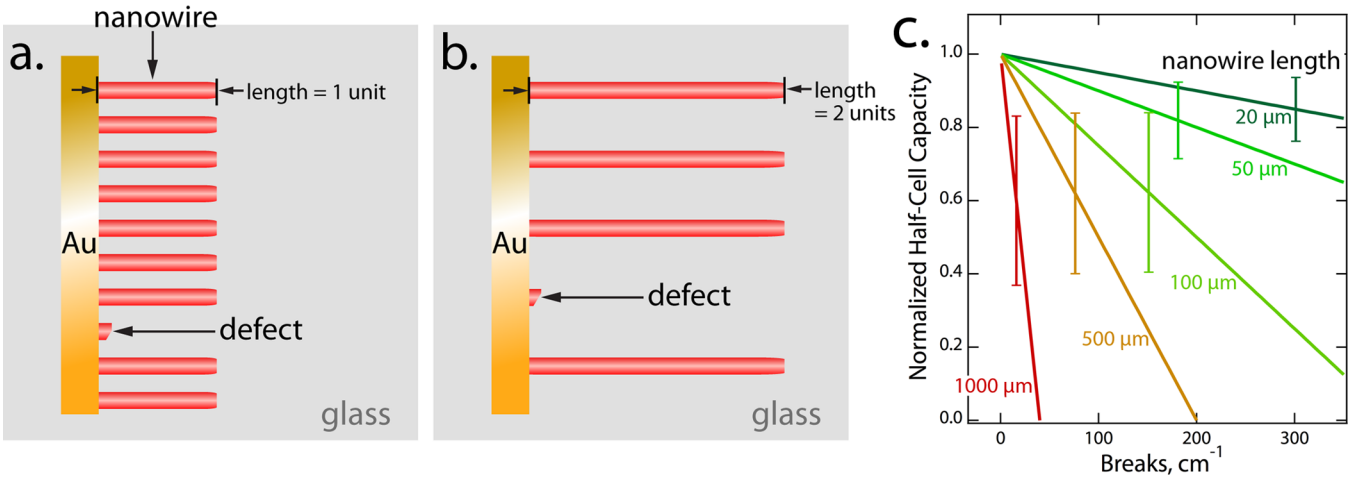

Figure 2. Capacitor electrodes based upon long nanowires are more susceptible to capacity loss resulting from nanowire breakage. (a) For example, the influence of a single break in a nanowire reduces the total (half-cell) capacity of this electrode by, at most, −10%. (b) For an array of nanowires that are twice as long, but having the same total length, the influence of a single break on the total capacity can be as high as −20%. Of course, the influence of a break will depend upon where along the length of the nanowire it occurs. (c) The influence of a broken nanowire on the capacity of a half-cell is larger as the length of the nanowires increases. For example, if the total length of nanowires in a half-cell is 1.0 cm, the total capacity, normalized to time = 0, is given by $1.0 - DL/2$, where D is the number of breaks present in the array of nanowires and L is the length of individual nanowires. This calculation assumes linear nanowires, not nanowire loops as employed here, for reasons of simplicity. The standard deviation of these traces is given by: $\sigma\ (cm) = DL/(2(12)^{1/2})$.

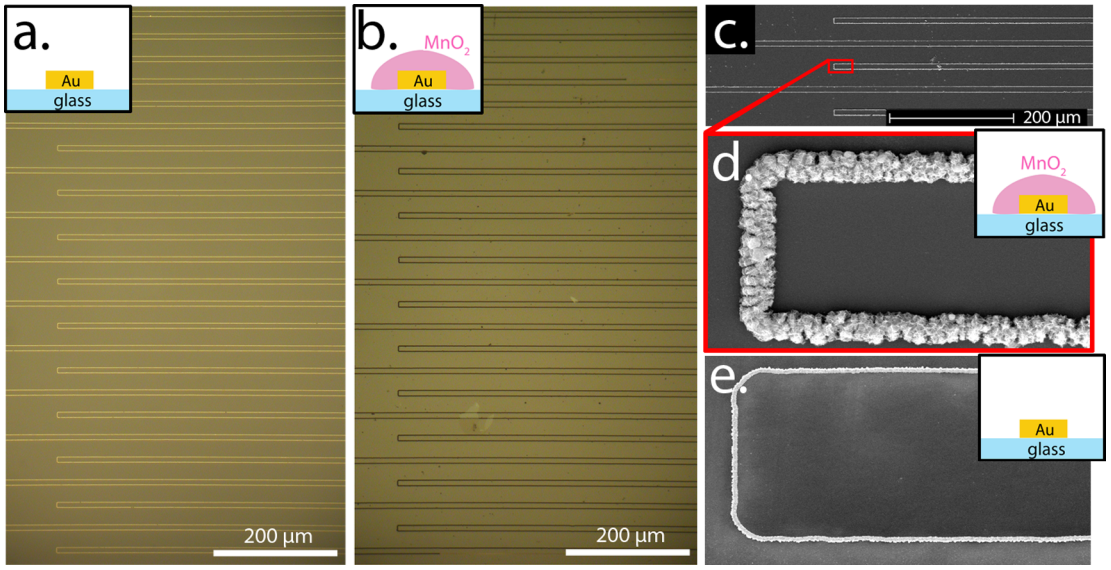

Figure 3. Micrographs of interdigitated nanowire capacitors. (a, b) Optical micrographs of an interdigitated gold nanowire array (a) and a Au@δ-MnO_2 nanowire array (b). A small section of the array is shown in these images. The total nanowire length was 2.5 mm. Scanning electron micrographs (c–e) show, in (c), nanowires at the same magnification seen in (a, b). Au@δ-MnO_2 (d) and gold-only nanowires (e) are also shown at higher magnification.

using a Princeton Applied research 2263 potentiostat. A Pt foil was used as counter electrode with a saturated mercurous sulfate reference electrode (MSE) for MnO_2 synthesis. The electrochemical characterizations were conducted in 1.0 M $LiClO_4$ (battery grade, dry, 99.99%) in dry acetonitrile with a two-electrode cell using a Gamry potentiostat. Prior to each measurement, the acetonitrile is presaturated with N_2 gas. Ultrapure, dry acetonitrile required for cycle life testing was prepared by processing reagent grade acetonitrile with a Jorg Meyer Phoenix SDS column purification system. $LiClO_4$ was battery grade from Sigma-Aldrich, with a purity of 99.99%.

Structural Characterization. Scanning electron micrographs were acquired using a Philips XL-30 FEG SEM (field emission gun scanning electron microscope) operated at 10 keV. All samples were sputtered with a thin layer of Au/Pd before imaging to prevent charging. Atomic force microscopy (AFM) images and amplitude traces were acquired using an Asylum Research, MFP-3D AFM equipped with Olympus, AC160TS tips in a laboratory air ambient.

RESULTS AND DISCUSSION

Preparation of Capacitors from Au@δ-MnO_2 Core@Shell Nanowires. The goal of this project is to evaluate the feasibility of preparing capacitors consisting of lithographically patterned and interdigitated nanowires that are ultralong (l = 5.0 mm) and to determine the charge storage performance available from such systems. In pursuit of this objective, we fabricated capacitors consisting of interdigitated nanowire hairpin-shaped loops (Figure 1a) where the length of the

dx.doi.org/10.1021/am500051d | ACS Appl. Mater. Interfaces 2014, 6, 5018–5025

nanowire contained within each loop was 2.5 mm and each device contained a total of 750 nanowire loops—375 for each plate of the capacitor. Other dimensions are as shown in Figure 1a. The δ-MnO_2 that is responsible for charge storage in these nanowires has a high electrical resistivity (0.20−100 Ω cm)[4] that presents a problem for the use of this material in battery electrodes.[6,7] Despite this issue, the use of MnO_2 nanowires with millimeter-scale lengths was enabled by a core@shell architecture in which a gold nanowire with lateral dimensions of 40 nm × 150−250 nm was conformally coated with a shell of δ-MnO_2 of thickness 68−220 nm. For these Au@δ-MnO_2 core@shell nanowires, the distance across which MnO_2 must conduct electrons is reduced to the thickness of the MnO_2 shell and the resulting Ohmic drop is expected to be negligible.

The fabrication of Au/MnO_2 core:shell nanowires using LPNE[14−16] has been previously described.[18] Briefly, the process flow for this fabrication (Figure 1) starts with the preparation of an array of gold nanowire loops on glass (Figure 1b, steps 1−6).[15] Each gold nanowire has a rectangular cross section with a height of 40 nm, a width of 150−250 nm, and a total length of 2.5 mm, and adjacent loops were spaced on the surface by 30 μm (Figure 1a). Then, using these gold nanowires as working electrodes, a conformal layer of δ-MnO_2 shell is electrodeposited (Figure 1b, step 7) by oxidation of a Mn^{2+} solution according to[20]

$$Mn^{2+} + 2H_2O + xLi^+ \rightarrow Li_x(Mn_x^{3+}Mn_{1-x}^{4+})O_2 + 4H^+ + (2-x)e^- \quad (2)$$

Previously, measurements of x for nanowires prepared using this procedure yields values in the range from 0.30 to 0.36.[17] Water is also incorporated into the MnO_2 structure during growth.[20] The structure of the resulting MnO_2 was confirmed as δ-phase by both the X-ray diffraction and Raman spectroscopy.[18]

At the magnification available in an optical microscope, gold nanowires look the same before (Figure 3a) and after (Figure 3b) MnO_2 deposition, except that the MnO_2-coated wires are darker. At the higher magnification afforded by SEM (Figure 3c), the formation of a cauliflower-like δ-MnO_2 shell (Figure 3d) on the gold nanowire (Figure 3e) can be clearly seen. Approximately 80% of the gold nanowires patterned on a device were encapsulated by MnO_2. The remaining 20% of the gold nanowires had sections that were not coated by MnO_2 because of the presence of breaks along the 2.5 mm length that compromised the electrical continuity of the gold nanowire current collector. An estimate of the MnO_2 shell thickness can be obtained from AFM measurements of the nanowire topography (Figure 4). The difference between the apparent height of nanowires measured by AFM and that of the gold core is the thickness of the electrodeposited MnO_2 shell.

The thickness of the MnO_2 shell can be controlled over the range from 60 to 300 nm based upon the deposition duration (Figure 5). The slope of this calibration plot depends critically on the number density of gold nanowires on the glass surface. For example, in our prior work,[18] we prepared Au@δ-MnO_2 beginning with gold nanowires that were patterned at 5 μm pitch, and for such arrays, 200 nm MnO_2 shells required a deposition duration of 20−25 s, whereas, in the present case (Figure 1a) where interwire spacings are either 10 or 35 μm, 200 nm MnO_2 shells are obtained in just 8 s (Figure 5). This observation provides evidence that, for the 5 μm spaced gold nanowires, adjacent wires are not operating independently of one another. Instead, flux-sharing of Mn^{2+} (eq 2) between adjacent nanowires is occurring.

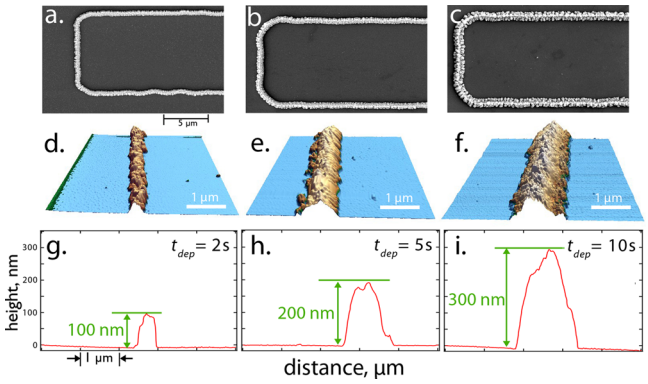

Figure 4. Adjusting the MnO_2 shell thickness. Scanning electron micrographs (SEM, a−c) and atomic force micrographs (AFM, d−f) of a single gold@δ-MnO_2 core@shell nanowire coated onto a gold nanowire with height = 43 nm. Shown here are Au@δ-MnO_2 prepared using electrodeposition times of 2 s (a, d, g), 5 s (b, e, h), and 10 s (c, f, i) that produced mean MnO_2 shell thicknesses of 121 ± 6 nm, 220 ± 9 nm, and 323 ± 17 nm, respectively. Height versus distance amplitude traces (g−i) are shown for the AFM images of (d)−(f).

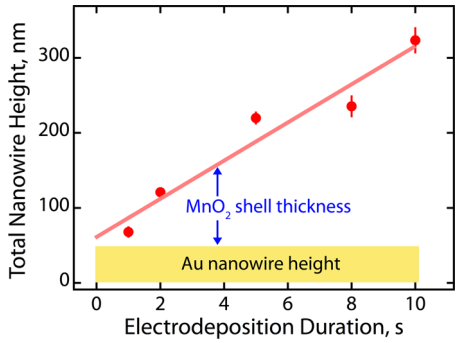

Figure 5. Total Au@δ-MnO_2 core@shell nanowire height and estimated MnO_2 shell thickness versus electrodeposition duration, measured using AFM.

Electrochemical Characterization of Capacitors. Two independent arrays of 375 Au@δ-MnO_2 nanowire loops comprise each capacitor (Figure 1a). The cyclic voltammetry (CV) of each of these two arrays was probed individually, in a three-electrode configuration, across a 0.60 V window at 100 mV/s (Figure 6a). These CVs are virtually identical and produce a C_{sp} = 226 and 228 F/g for the two arrays, based upon the equation

$$C_{sp} = \frac{Q}{\Delta E \times m} \quad (3)$$

where Q is the total charge associated with scanning from −0.40 to +0.20 V, ΔE is 0.6 V, and m is the dry mass of the MnO_2. To obtain m from the deposition charge with high precision, we conducted[18] a quartz crystal microbalance (QCM) gravimetry study to determine the Coulombic efficiency of MnO_2 electrodeposition. The similarity of the CVs for the two half-cells implies that the number of defects resulting in broken nanowires is close to identical in these two arrays. In prior work, we found that shorter (≈1 mm) Au@δ-MnO_2, linear core@shell nanowires with a shell thickness of 68(±3) nm produced a somewhat higher C_{sp} of 450(±70) F/g at 100 mV/s.[18]

dx.doi.org/10.1021/am500051d | ACS Appl. Mater. Interfaces 2014, 6, 5018−5025

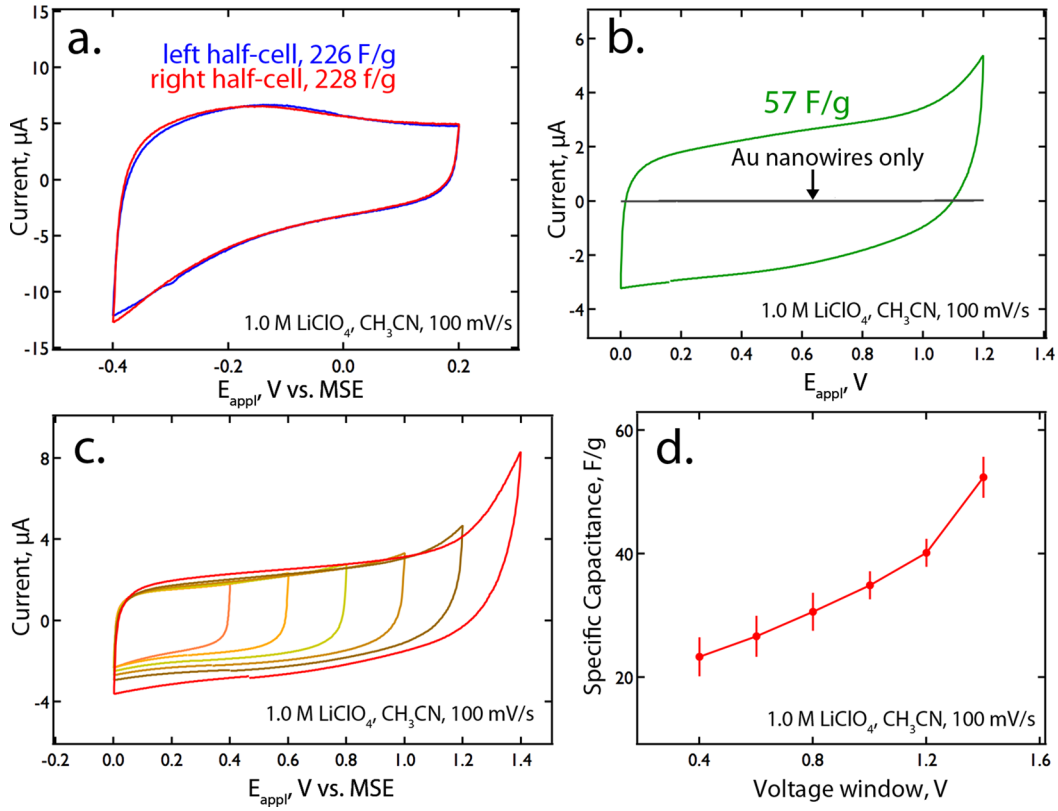

Figure 6. Electrochemical capacitor characterization. Shown here are data for a symmetrical interdigitated supercapacitor (as shown in Figure 1a) consisting of identical interdigitated gold:δ-MnO_2 core:shell nanowires having a MnO_2 shell thickness of 121 ± 6 nm. (a) Cyclic voltammograms (CVs, at 100 mV/s) of both half-cells versus MSE reference electrode in a three-electrode cell. C_{sp} values of 226 and 228 F/g are obtained. (b) CVs (100 mV/s) of the same two half-cells versus one another (green). The measured C_{sp} is 57 F/g. Also shown here are CVs for the gold nanowire current collector alone (lateral dimensions: 43 nm (h) × 200 nm (w)) (black). (c) Six CVs illustrating the influence of scan window—ranging from 0.40 to 1.4 V—on C_{sp}. (d) Plot of C_{sp} versus scan window size.

By operating the two nanowire array half-cells in a two-electrode configuration, the C_{sp} of the capacitor can be measured. In this case, Q in eq 3 is the total charge in a 1.2 V scanning window, and m is the sum of the dry mass of MnO_2 deposited on both sides of the gold nanowire electrodes (Figure 6b, green trace). We observe a C_{sp} of 57 F/g in this case—very close to one-fourth the value for the two individual electrodes, as predicted based upon the series combination of the two identical nanowire capacitors, and the fact that the total mass of MnO_2 in the system is doubled.

An operational voltage window of 1.2 V is the largest that supports reversible charge storage in this system. This can be seen by acquiring CVs using windows of 0.4, 0.6, 0.8, 1.0, 1.2, and 1.4 V (Figure 6c). Both the differential capacitance at any potential (Figure 6c) and the integrated C_{sp} increased over this range (Figure 6d), but we found that the cycle stability of the system was reduced for windows larger than 1.2 V. This irreversibility is anticipated from the irreversible Faradaic process that is seen at polarizations above 1.2 V in the CVs of Figure 6c.

Using 1.2 V as the total polarization window, excellent cycle stability for this capacitor is obtained from cycle 20 to 4000 (Figure 7a,b) with a 10% loss in capacity from 4000 to 6000 cycles. The origin of the rapid decrease in C_{sp} during the first 20 cycles is unclear. SEM images (Figure 7c,d) reveal that the MnO_2 shell develops fissures after 6000 cycles. These cracks may signal the delimitation of the MnO_2 shell from the gold nanowire core, possibly accounting for loss of capacity after 4000 cycles. More work will be required to definitively assess the origin and influence of these defects on nanowire performance. However, the morphological changes seen in Figure 7d are not seen at earlier junctures and are presumably not responsible for the loss of C_{sp} in the first 20 cycles.

Galvanostatic charging/discharging curves were acquired for nanowire capacitors with three different MnO_2 shell thicknesses (e.g., Figure 8a). The maximum power density, P_{max}, and energy density, E_{max}, were calculated from these data according to[21,22]

$$P_{max} = \frac{V^2}{4Rm} \text{ (kW/kg)} \quad (4)$$

$$E_{max} = \frac{1}{2}CV^2 \text{ (Wh/kg)} \quad (5)$$

where V is the potential window, excluding the iR drop, R is the equivalent series resistance (ESR) determined from the iR drop, V_{iR}, m is the total mass of MnO_2 at both electrodes, and C is the total capacitance.[21−24] R is obtained from $R = \Delta V_{iR}/2i$, and C is obtained from the initial slope of the discharge curve, $C = i(-\Delta V/\Delta t)$ (Figure 8b). The value for R was taken to be the average measured for five charge/discharge rates varying from 1 to 15 A/g.

Ragone plots (Figure 8b) show data for three nanowire capacitors with MnO_2 shell thicknesses of 68 (±8) nm, 121 (±6) nm, and 220 (±9) nm. P_{max} (165 kW/kg) and E_{max} (24 Wh/kg) are both highest for nanowires with the 68 nm shell.

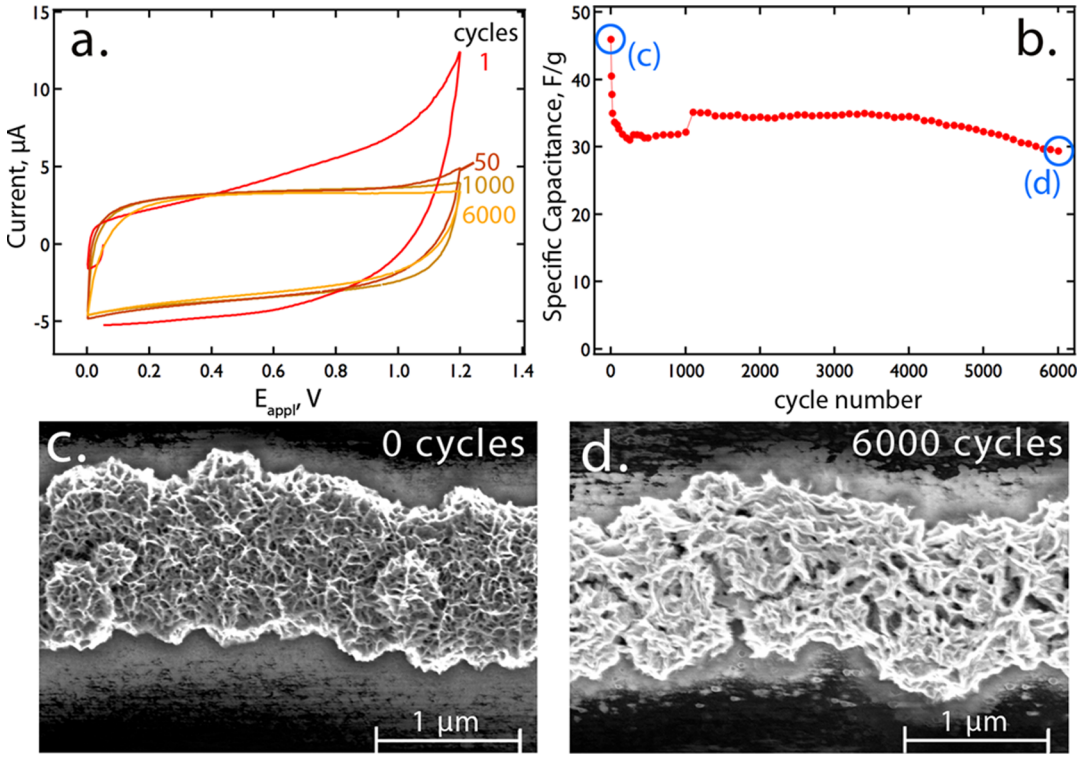

Figure 7. Assessment of cycle stability of C_{sp} for Au@δ-MnO_2 core:shell nanowire capacitors. (a) Cyclic voltammograms (100 mV/s) for a symmetric supercapacitor showing cycles 1, 50, 1000, and 6000. Au@δ-MnO_2 core:shell nanowires had a MnO_2 shell thickness of 220 ± 9 nm. Data in this figure were acquired in 1.0 M $LiClO_4$ prepared with ultradry acetonitrile. (b) C_{sp} at 100 mV/s versus cycle number for 1.2 V cycles as shown in (a). (c, d) SEM images of (c) an as-prepared Au@δ-MnO_2 core:shell nanowire, before the initial 20 conditioning cycles, and (d) an identical nanowire after 6000 cycles. The images shown in (c) and (d) were obtained without metal coating the sample so some charging is apparent in these images.

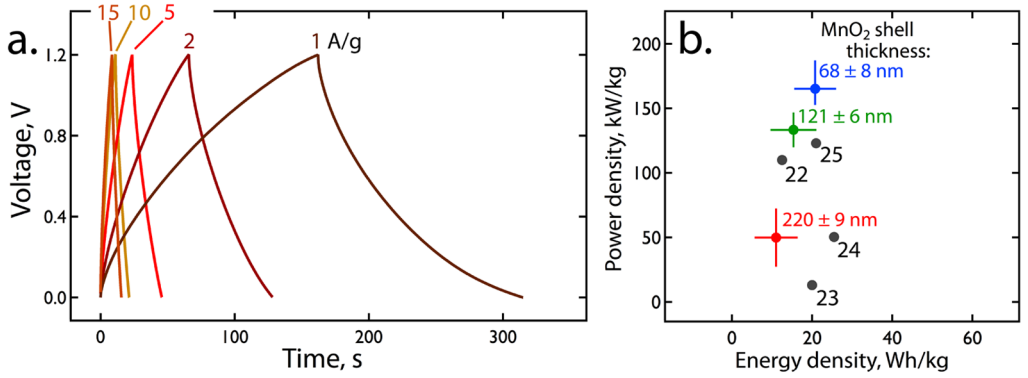

Figure 8. (a) Galvanostatic charge/discharge curves for interdigitated Au@δ-MnO_2 core:shell nanowire capacitors. Shown are traces for rates of 1, 2, 5, 10, and 15 A/g for a MnO_2 shell thickness of 68 (±8) nm. (b) Ragone plot of power density versus energy density at a 1 A/g charge/discharge rate for three nanowire capacitors with MnO_2 shell thicknesses of 68 (±8) nm, 121 (±6) nm, and 220 (±9) nm. An increase in rate from 1 to 15 A/g reduced E_{max} by 30−35% for all MnO_2 shell thicknesses (e.g., to 16 Wh/kg from 24 Wh/kg for nanowires with a 68 nm shell). Black data points represent literature values.[22−25]

These parameters are only marginally lower for the 121 nm shell, and significantly lower for the thickest shell of 220 nm. It is also apparent (Figure 8b) that the MnO_2 shell thickness exerts a much stronger influence on P_{max} than on E_{max}. This behavior is commensurate with our prior investigations of Au@δ-MnO_2 core:shell nanowires in three-electrode measurement systems.[17]

Importantly, P_{max} values for a rate of 1 A/g at the 68 and 121 nm nanowires exceed the highest measured values for symmetrical MnO_2 capacitor systems[23] and also several recent asymmetrical capacitors in which one electrode is MnO_2.[22,24,25]

Measured values of E_{max} equal that measured in all but one prior study. Literature benchmarks are shown in Figure 8b, labeled by reference number. Cui and co-workers[23] obtained P_{max} = 13 kW/kg and E_{max} = 4−17 Wh/kg for textile fiber/carbon nanotube/MnO_2 symmetrical capacitors. Bao et al.[22] prepared hybrid textile fiber/graphene/MnO_2 asymmetrical capacitors that yielded P_{max} = 110 kW/kg and E_{max} = 12.5 Wh/kg. Asymmetrical all-nanowire capacitors fabricated by Zhou et al.,[24] consisting of MnO_2-coated carbon nanotubes and In_2O_3-coated carbon nanotubes, produced P_{max} = 50.3 kW/kg and E_{max} = 25.5 Wh/kg—a much smaller P_{max} and slightly higher

dx.doi.org/10.1021/am500051d | ACS Appl. Mater. Interfaces 2014, 6, 5018−5025

E_{max} value as compared with our 68 nm shell system. Finally, P_{max} = 123 kW/kg and E_{max} = 21 Wh/kg were seen for an asymmetrical MnO_2/activated carbon composite electrode material by Béguin and co-workers.[25] We are not aware of other studies achieving still higher power or energy metrics than those summarized here. It is important to note, however, that the volumetrically and gravimetrically normalized power and energy that include the glass slides on which these nanowire-based capacitors are deposited will be very low, both as a consequence of low fill factors for the horizontal nanowire device architectures and because of the significant mass of these slides relative to the nanowire electrodes. For this reason, we expect horizontal nanowire systems to be of value primarily for fundamental investigations of nanowire performance, such as investigations of the mechanisms contributing to degradation and failure in these systems.

CONCLUSIONS

The main conclusion of this work is that horizontal all-nanowire capacitor systems prepared by LPNE are capable of producing state-of-the-art power and energy,[22−25] specifically, values for P_{max} (165 kW/kg) and E_{max} (24 Wh/kg) for nanowires with the 68 nm MnO_2 shell. A cycle life of up to 6000 cycles is competitive with prior work on similar systems.[22−25] This performance is all the more surprising when it is considered that, in principle, capacitors that incorporate ultralong nanowires should have a higher susceptibility to capacity fade caused by failure modes that cause breakage of the nanowires (Figure 2). After an initial conditioning period of 20 cycles, a high degree of cycle stability was also observed to 6000 times at 100 mV/s across a 1.2 V window. These data support the conclusion that durable, ultrahigh power density capacitors can be fabricated based upon millimeter-scale metal core−metal oxide shell nanowire arrays.

AUTHOR INFORMATION

Corresponding Author

*E-mail: rmpenner@uci.edu.

Notes

The authors declare no competing financial interest.

ACKNOWLEDGMENTS

This material is based upon work supported as part of the Nanostructures for Electrical Energy Storage, an Energy Frontier Research Center funded by the U.S. Department of Energy, Office of Science, Office of Basic Energy Sciences, under Award Number DESC0001160. Valuable discussions with Professor Phil Collins and Brad Corso are gratefully acknowledged. Electron microscopy and powder X-ray diffraction were carried out in the Laboratory for Electron and X-ray Instrumentation (LEXI) at University of California, Irvine.

REFERENCES

(1) Conway, B. Transition from Supercapacitor to Battery Behavior in Electrochemical Energy Storage. *J. Electrochem. Soc.* **1991**, *138*, 1539−1548.

(2) Conway, B. *Electrochemical Supercapacitors: Scientific Fundamentals and Technological Applications (POD)*; Kluwer Academic/Plenum: New York, 1999.

(3) Simon, P.; Gogotsi, Y. Materials for Electrochemical Capacitors. *Nat. Mater.* **2008**, *7*, 845−854.

(4) Klose, P. Electrical Properties of Manganese Dioxide and Manganese Sesquioxide. *J. Electrochem. Soc.* **1970**, *117*, 854−858.

(5) Wei, W.; Cui, X.; Chen, W.; Ivey, D. G. Manganese Oxide-Based Materials as Electrochemical Supercapacitor Electrodes. *Chem. Soc. Rev.* **2011**, *40*, 1697−1721.

(6) Rolison, D. R.; Long, R. W.; Lytle, J. C.; Fischer, A. E.; Rhodes, C. P.; McEvoy, T. M.; Bourga, M. E.; Lubers, A. M. Multifunctional 3D Nanoarchitectures for Energy Storage and Conversion. *Chem. Soc. Rev.* **2009**, *38*, 226−252.

(7) Long, J.; Dunn, B.; Rolison, D.; White, H. Three-Dimensional Battery Architectures. *Chem. Rev.* **2004**, *104*, 4463−4492.

(8) Whittingham, M. Lithium Batteries and Cathode Materials. *Chem. Rev.* **2004**, *104*, 4271−4301.

(9) Jiang, H.; Zhao, T.; Ma, J.; Yan, C.; Li, C. Ultrafine Manganese Dioxide Nanowire Network for High-Performance Supercapacitors. *Chem. Commun.* **2011**, *47*, 1264−1266.

(10) Xia, H.; Feng, J.; Wang, H.; Lai, M. O.; Lu, L. MnO_2 Nanotube and Nanowire Arrays by Electrochemical Deposition for Supercapacitors. *J. Power Sources* **2010**, *195*, 4410−4413.

(11) Xu, C.; Zhao, Y.; Yang, G.; Li, F.; Li, H. Mesoporous Nanowire Array Architecture of Manganese Dioxide for Electrochemical Capacitor Applications. *Chem. Commun.* **2009**, 7575−7577.

(12) Xiao, W.; Xia, H.; Fuh, J. Y. H.; Lu, L. Growth of Single-Crystal α-MnO_2 Nanotubes Prepared by a Hydrothermal Route and Their Electrochemical Properties. *J. Power Sources* **2009**, *193*, 935−938.

(13) Chen, S.; Zhu, J.; Han, Q.; Zheng, Z.; Yang, Y.; Wang, X. Shape-Controlled Synthesis of One-Dimensional MnO_2 via a Facile Quick-Precipitation Procedure and Its Electrochemical Properties. *Cryst. Growth Des.* **2009**, *9*, 4356−4361.

(14) Xiang, C.; Yang, Y.; Penner, R. M. Cheating the Diffraction Limit: Electrodeposited Nanowires Patterned by Photolithography. *Chem. Commun.* **2009**, 859−873.

(15) Xiang, C.; Kung, S.-C.; Taggart, D. K.; Yang, F.; Thompson, M. A.; Gueell, A. G.; Yang, Y.; Penner, R. M. Lithographically Patterned Nanowire Electrodeposition: A Method for Patterning Electrically Continuous Metal Nanowires on Dielectrics. *ACS Nano* **2008**, *2*, 1939−1949.

(16) Menke, E. J.; Thompson, M. A.; Xiang, C.; Yang, L. C.; Penner, R. M. Lithographically Patterned Nanowire Electrodeposition. *Nat. Mater.* **2006**, *5*, 914−919.

(17) Yan, W.; Ayvazian, T.; Kim, J.; Liu, Y.; Donavan, K. C.; Xing, W.; Yang, Y.; Hemminger, J. C.; Penner, R. M. Mesoporous Manganese Oxide Nanowires for High-Capacity, High-Rate, Hybrid Electrical Energy Storage. *ACS Nano* **2011**, *5*, 8275−8287.

(18) Yan, W.; Kim, J. Y.; Xing, W.; Donavan, K. C.; Ayvazian, T.; Penner, R. M. Lithographically Patterned Gold/Manganese Dioxide Core/Shell Nanowires for High Capacity, High Rate, and High Cyclability Hybrid Electrical Energy Storage. *Chem. Mater.* **2012**, *24*, 2382−2390.

(19) Ataherian, F.; Wu, N.-L. Long-Term Charge/Discharge Cycling Stability of MnO_2 Aqueous Supercapacitor under Positive Polarization. *J. Electrochem. Soc.* **2011**, *158*, A422−A427.

(20) Nakayama, M.; Kanaya, T.; Lee, J.-W.; Popov, B. N. Electrochemical Synthesis of Birnessite-Type Layered Manganese Oxides for Rechargeable Lithium Batteries. *J. Power Sources* **2008**, *179*, 361−366.

(21) Brousse, T.; Toupin, M.; Belanger, D. A Hybrid Activated Carbon-Manganese Dioxide Capacitor Using a Mild Aqueous Electrolyte. *J. Electrochem. Soc.* **2004**, *151*, A614−A622.

(22) Yu, G.; Hu, L.; Vosgueritchian, M.; Wang, H.; Xie, X.; McDonough, J. R.; Cui, X.; Cui, Y.; Bao, Z. Solution-Processed Graphene/MnO_2 Nanostructured Textiles for High-Performance Electrochemical Capacitors. *Nano Lett.* **2011**, *11*, 2905−2911.

(23) Hu, L.; Chen, W.; Xie, X.; Liu, N.; Yang, Y.; Wu, H.; Yao, Y.; Pasta, M.; Alshareef, H. N.; Cui, Y. Symmetrical MnO_2−Carbon Nanotube−Textile Nanostructures for Wearable Pseudocapacitors with High Mass Loading. *ACS Nano* **2011**, *5*, 8904−8913.

(24) Chen, P.-C.; Shen, G.; Shi, Y.; Chen, H.; Zhou, C. Preparation and Characterization of Flexible Asymmetric Supercapacitors Based on

Transition-Metal-Oxide Nanowire/Single-Walled Carbon Nanotube Hybrid Thin-Film Electrodes. *ACS Nano* **2010**, *4*, 4403−4411.
(25) Beguin, F.; Khomenko, V.; Raymundo-Pinero, E. Optimisation of an Asymmetric Manganese Oxide/Activated Carbon Capacitor Working at 2 V in Aqueous Medium. *J. Power Sources* **2006**, *153*, 183−90.